THE JOURNAL OF PHYSICAL CHEMISTRY C

Article

pubs.acs.org/JPCC

Doped Perovskites To Evaluate the Relationship between Fuel–Oxidizer Thermite Ignition and Bond Energy, Electronegativity, and Oxygen Vacancy

Xizheng Wang,[†] Tao Wu,[†] and Michael R. Zachariah*[,†,‡]

[†]Department of Chemistry and Biochemistry and [‡]Department of Chemical and Biomolecular Engineering, University of Maryland, College Park, Maryland 20742, United States

Supporting Information

ABSTRACT: Despite our knowledge of the existence of the violent thermite reaction for over 100 years, it is still not yet understood how the properties of a metal oxide oxidizer relate to and influence the ignition temperature. To address this shortcoming, we prepared a series of perovskite-based oxidizers which enable a systematic investigation of how materials properties of the oxidizer relate to the ignition temperature. In this paper, nine lanthanum-based perovskites with different Sr^{2+} doping of the A-site and different B-site transition metals were synthesized. The perovskite O_2 release and ignition temperatures with aluminum were measured by fast heating (>10^5 K/s) temperature-jump/time-of-flight mass spectrometry coupled with high-speed imaging. These results were then correlated with the average bond energy and overall metal–oxygen electronegativity difference. Remarkably, we found a linear relationship between average bond energy and electronegativity with ignition temperature. To our knowledge this is the first demonstration of the connection between metal–oxygen bond energy, electronegativity, and ignition temperature.

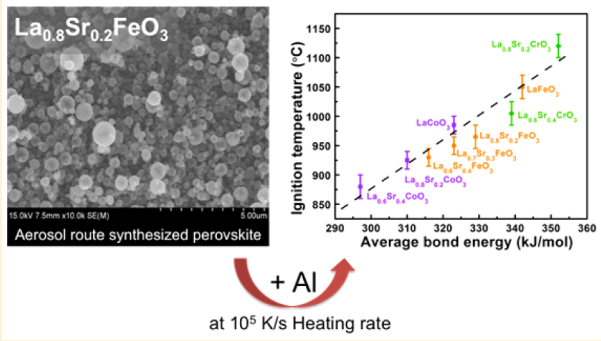

INTRODUCTION

The thermite reaction[1] has been exploited for well over 100 years and involves the violent reaction between a metallic fuel (e.g., Al, Fe, etc.) and a metal oxide oxidizer (e.g., CuO, Bi_2O_3, etc.). More recently with the interest in nanoscale materials, the thermite reaction has generated renewed interest, as the reduced length scale offers the potential to significantly reduce the energy release time (<1 ms).[2−4] By far the most commonly employed fuel is Al due to the high enthalpy of reaction and its ready availability.[5,6] Despite our knowledge of this seemingly simply oxygen exchange reaction, the rapidity of the reaction has made it difficult to understand it mechanistically.[7]

Substantial effort has been devoted to studying the mechanism and parameters that govern the initiation reaction between nano aluminum and metal oxide. The most direct measure of the onset of runaway violent reaction is the ignition temperature. For metallic fuels, for example aluminum, there is a naturally occurring thin Al_2O_3 shell (~2−5 nm), which prevents direct contact between aluminum and metal oxide.[8,9] It is generally believed that the prerequisite for ignition is the existence of molten aluminum.[10,11] However, Stamatis et al.[12] reported the ignition temperature of Al/MoO_3 is lower than the melting point of aluminum (633 °C) resulting from amorphous alumina to a crystalline polymorph (~500 °C). Dean et al. examined the Al–NiO system and found a much lower ignition temperature (~400 °C) than either the melting point of aluminum or the decomposition temperature of NiO,[13] indicating it is a condensed phase reaction. Sullivan et al.[14] proposed Al/WO_3 undergoes a reactive sintering mechanism, whereby initiation of the reaction occurs only when condensed-phase reactants have an interfacial contact. In fact, the most recent evidence points to metal–metal oxide reactions initiating through a condensed phase reaction,[15−18] even though the bulk of the remaining chemistry might propagate through gas–solid processes. Jian et al. tried to correlate ignition temperature with gaseous oxygen released from the decomposition of metal oxide,[19] but the results showed that there can be large differences in ignition temperatures among different nano thermite formulations involving aluminum and metal oxides. In part, the challenge is that ignition is affected by experimental parameters, e.g., heating rate, experimental configuration, particle size, and packing. Studies show that thermite ignition depends on heating rate.[14,20,21] To better study thermite ignition, which by its nature is an extremely fast self-heating process, it is necessary to employ heating rates that more closely resemble self-heating rates (>10^5 °C/s).[15,16,19] In particular, ignition is a very different process than steady reaction. Ignition becomes self-sustaining when the self-heating rate overcomes the inherent heat loss process and thus cannot be evaluated at low heating rates.

Received: October 20, 2016
Revised: November 23, 2016
Published: November 28, 2016

DOI: 10.1021/acs.jpcc.6b10571
J. Phys. Chem. C 2017, 121, 147−152

However, even for seemingly the same experimental configuration (heating rate, experimental configuration), we have found that the ignition temperatures do not correlate with overall thermite reaction enthalpy as shown in Figure S1 for a range of common oxidizers. In summary, when we consider the totality of the research into initiation of metal−metal oxide redox reaction to the point of ignition, we still cannot say what fundamental properties of the oxidizer determine the ignition point.

In part, the problem is due to the large number of variables comprising an oxidizer that might impact ignition, including bond energy, oxygen mobility, crystal structure, reaction interface area, thermal conductivity, heat capacity, and thermal contact, etc. In order to deal with this complexity, a system is needed in which most of the dependent variables can be held constant. One such class of material that offers the opportunity for such a study is perovskites.

Perovskite oxides, generally formularized as ABO_3, have been employed in solid oxide fuel and electrolysis cells (SOFC/SOEC),[22,23] heterogeneous catalysis of hydrocarbon,[24] membranes for oxygen separation,[25] and chemical looping combustion as oxygen carriers[26,27] due to their high oxygen reactivity and superior oxygen transport capacities. One of the main advantages of the perovskite structure is the possibility of adopting a large number of different A- and B-site cations or through partial substitution a wide range of combinations to adjust the redox properties. Thus, perovskites offer the opportunity to tweeze out from a microscopic prospective structure−function relationship relevant to oxidation of a fuel.

In this paper, we explored the role of oxygen transport properties, which are related to oxygen vacancy concentration, metal−oxygen bond energy, and electronegativity on ignition temperature with nano aluminum. More specifically, we evaluated the ignition behavior of a range of perovskites, synthesized by aerosol spray pyrolysis, chosen so as to enable systematic changes to the oxygen vacancy concentrations and bond energy by (a) substituting Sr^{2+} and/or (b) changing the B-site transition metal. The key to this study was to make these changes while maintaining the same crystal structure, particle morphology, and size of the perovskites. Our results show a very clear connection that elevated oxygen vacancy concentration, smaller average bond energy, and smaller electronegativity difference lower the ignition temperature.

EXPERIMENTAL SECTION

Synthesis of Perovskite. All perovskites were synthesized by aerosol spray pyrolysis[28] from metal nitrate aqueous solutions formulated with the desired metal ratios. $La(NO_3)_3 \cdot 6H_2O$ (≥99.0% pure), $Sr(NO_3)_3$ (≥99.0% pure), $Co(NO_3)_2 \cdot 6H_2O$ (≥98% pure), $Cr(NO_3) \cdot 9H_2O$, and $Fe(NO_3) \cdot 9H_2O$ were obtained from Sigma-Aldrich and pyrolyzed at 1050 °C with a residence time of about 1 s to obtain $LaBO_3$ (B = Cr, Fe, Co), $La_{0.8}Sr_{0.2}BO_{3-\delta}$ (B = Cr, Fe, Co), and $La_{0.6}Sr_{0.4}BO_{3-\delta}$ (B = Cr, Fe, Co). For instance, in order to synthesize $LaCoO_3$, a 0.2 mol/L precursor solution, containing stoichiometric $La(NO_3)_3$, $Co(NO_3)_3$ was atomized by a nebulizer to generate nominally 1 μm droplets with compressed air. The atomized droplets flowed through a diffusion dryer, where most of the water was absorbed, leaving solid precursor particles which were then passed to a tubular furnace to produce the desired perovskite particles. The final product was collected on a Millipore membrane with a pore size of 0.4 μm.

Synthesis of Al/Perovskite Thermite Compositions. Nano aluminum particles (~50 nm) were purchased from Novacentrix Corporation. To prepare the thermite composite, stoichiometric mixtures of nano aluminum and perovskite were mixed and then sonicated in hexane for 30 min. For control of stoichiometry, the Al_2O_3 shell (19% of the mass) content in nano aluminum was accounted for.

Materials Characterization. The crystal structures of the synthesized perovskites were characterized by X-ray diffraction (XRD) performed on a Bruker D8 diffractometer with Cu Kα radiation. Le Bail refinement of all diffraction patterns was performed with the TOPAS 4.2 software.[29] The morphologies of the perovskites were measured by scanning electron microscopy (SEM) conducted on a Hitachi SU-70 instrument. Size distributions were obtained by measuring 300 individual nanoparticles statistically from SEM images of each sample, using Nano Measurer 1.2 image analysis software. The morphologies and elemental analysis of thermite powders were measured by SEM equipped with energy dispersive X-ray spectroscopy (EDS).

Oxygen Release Measurement from Perovskites. Oxygen release temperatures (in the absence of fuel) from individual oxidizer, perovskites, were measured with temperature-jump/time-of-flight mass spectrometry (T-Jump/TOFMS).[30,31,19] A hexane suspension of perovskite powders was droppered onto a 70 μm diameter platinum filament and allowed to air-dry. The platinum wire can be joule heated at a rapid rate ~4×10^5 °C/s to ~1300 °C within 3 ms. The filament was directly inserted into the ionization region of a TOFMS, where the gaseous products could be temporally analyzed. The temperature of the wire was determined from electric resistance based on the Callendar−Van Dusen equation, through a simultaneous measure of temporal applied voltage and current. The ionization/extraction region of the TOFMS was pulsed at 10 kHz, resulting in a full mass spectrum every 100 μs. A 600 MHz digital oscilloscope was used for data acquisition with a sampling rate of 100 megasamples/s.

Because of the size of nanoparticles compared with the wire and based on our previous result, the temperature of the wire is essentially equal to the temperature of the oxidizer system.[32] The temperature of the wire corresponding to the initial release of O_2 was regarded as the O_2 release temperature of perovskites.

Ignition Temperature Measurement of Thermites. The ignition temperature was also measured in the T-Jump/TOFMS using direct optical emission with a high-speed camera (Vision Research Phantom v12.0) operating at 67 056 frames/s. The experiment is equivalent to the oxygen release measurement with the exception of the presence of the fuel. Ignition was determined as the onset of optical emission.

RESULTS AND DISCUSSION

Structure and Morphology. Figure 1 shows XRD patterns for each synthesized $LaBO_3$ (B = Cr, Fe, Co), $La_{0.8}Sr_{0.2}BO_{3-\delta}$ (B = Cr, Fe, Co), and $La_{0.6}Sr_{0.4}BO_{3-\delta}$ (B = Cr, Fe, Co). We find that all the synthesized perovskites are pseudocubic, belonging to either cubic (*Pm*-3*m*), orthorhombic (*Pnma*), or rhombohedral ($R\bar{3}c$) space groups. Table S1 and Figure S2 present the refined results from Le Bail fitting, performed with the TOPAS 4.2 software. Although minor amounts of impurities peaks were found for $La_{0.6}Sr_{0.4}CrO_{3-\delta}$, the perovskite phase dominates. In the BO_6 octahedron the transformation from cubic (*Pm*-3*m*) to orthorhombic (*Pnma*) leads to a

DOI: 10.1021/acs.jpcc.6b10571
J. Phys. Chem. C 2017, 121, 147−152

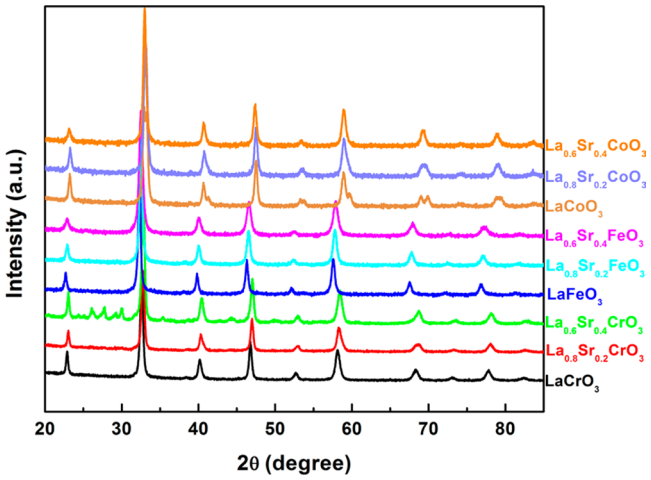

Figure 1. X-ray diffraction patterns of aerosol spray synthesized doped perovskite, with their space groups listed in Table S1.

symmetry decrease, while the rhombohedral $R\bar{3}c$ involves the slight rotation of the BO_6 octahedron with respect to the cubic structure. Compared to the perfect cubic, these distortions of either orthorhombic or rhombohedral structure are slight,[33] and the coordinations of oxygen with A-site cation and B-site cation are maintained. Thus, it is reasonable to say all perovskites in this study have essentially the same crystal structure, and any slight difference should not have a controlling impact on ignition.

Figure 2 shows SEM images of (a) $LaFeO_3$, (b) $La_{0.8}Sr_{0.2}FeO_3$, and (c) $LaCrO_3$ (as-synthesized) representative powders, indicating essentially the same particle size distribution. The diameter of the particles should be log-normally distributed corresponding to the original spray size distribution. The size distribution of those representative particles measured from SEM images and the log-normal fit profile are shown in Figure S3, and the log-normal fit parameters are listed in Table S2. All samples have similar narrow log-normal distribution with $\sigma = 0.408 \pm 0.06$, and the average diameter is 115−126 nm. This result is consistent with our previous results that products have the same size distribution when synthesized under the same conditions (precursor concentration, flow rate, etc.).[34] Thus, in this study, there are no morphology differences between particles that warrant consideration. Figure S4 shows the representative SEM and EDS results for Al/$LaFeO_3$ and Al/$La_{0.6}Sr_{0.2}FeO_3$, indicating that the aluminum and perovskite particles are well mixed with many points of intimate contact between fuel and oxidizer.

Oxygen Release Temperature and Ignition Temperature. Before we consider fundamental parameters, we present two important measurables: the ignition temperature and the gaseous oxygen release temperature of the neat perovskite. The observed oxygen release temperature from the neat oxidizer and the observed ignition temperature of Al/perovskites, measured by T-Jump/TOFMS[35] coupled with a high-speed camera, are shown in Figure 3. What this result shows is that all

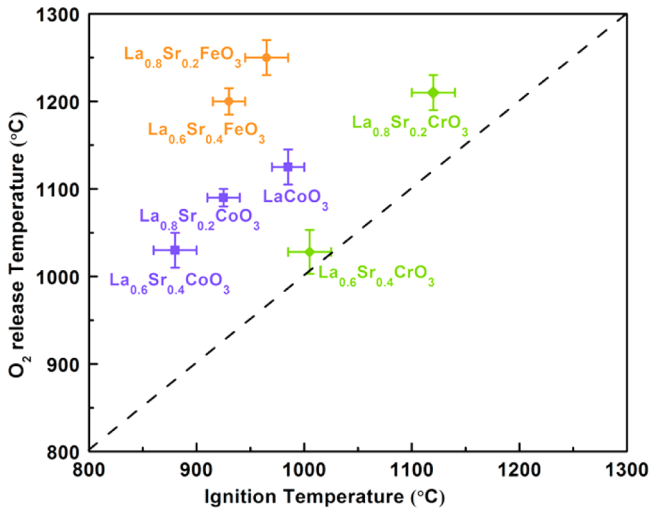

Figure 3. Oxygen release temperature from the perovskites vs ignition temperature for Al/perovskites indicates that ignition occurs prior to oxygen release (i.e., condensed state reaction).

data points lie above the diagonal, indicating that ignition occurs before oxygen (O_2) is released into the gas phase by the perovskite. Further for the temperature regime that T-jump/TOFMS could reach (~1350 °C), no O_2 release of $LaCrO_{3-\delta}$ and $LaFeO_{3-\delta}$ and no ignition of $LaCrO_{3-\delta}$ were observed. The time-resolved mass spectra of neat $LaCoO_3$ and $LaFeO_3$ under T-jump heating are shown in Figure S5 as examples.

The results from Figure 3 demonstrate that since ignition occurs at a temperature below which oxygen is evolved from the oxidizer, we must conclude the reaction takes place by condensed state redox reaction rather than gas evolution of oxygen leading to subsequent reaction with aluminum.

Bond Energy and Oxygen Vacancy Effects on Ignition. Numerous studies have focused on the defect chemistry and oxygen ion diffusion in perovskite oxides and their impact on redox properties[36−40] but have not been attempted for the thermite reaction. Prior works by others and us[19,41,42] show a relatively wide range of ignition temperatures for the same fuel, implying an oxidizer control mechanism. We thus begin presumptively with the conjecture that oxygen ion transport of these systematic perovskites affects the ignition temperature.

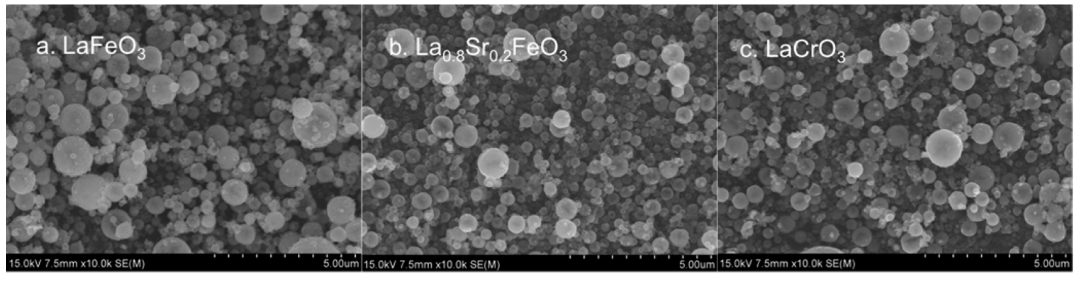

Figure 2. SEM images of as-synthesized (a) $LaFeO_3$, (b) $La_{0.8}Sr_{0.2}FeO_3$, and (c) $LaCrO_3$ as representative powders.

DOI: 10.1021/acs.jpcc.6b10571
J. Phys. Chem. C 2017, 121, 147−152

Oxygen ion transport, typically characterized by the ionic conductivity, can be related to the charge of the ion, Zq (O^{2-} in this case), the carrier mechanical mobility, μ, and the oxygen vacancy concentration, $[V_O^{\cdot\cdot}]$, through eq 1.

$$\sigma = Zq[V_O^{\cdot\cdot}]\mu \quad (1)$$

The use of perovskites is employed to:

a. Change Oxygen Vacancy Concentration by Doping with Sr^{2+}. Charge balance requires that substitution of Sr^{2+} for La^{3+} in the A-site leads to oxygen vacancies.

b. Change Oxygen Ion Mobility by Doping Sr^{2+} and Varying B-Site Metal Ion (Co^{3+}, Fe^{3+}, and Cr^{3+}). Previous research has found that oxygen ion mobility depends on the activation energy for oxygen ion migration,[43] which can be associated with an average bond energy (ABE) in the perovskite lattice.[44,45] By doping Sr^{2+} and varying the B-site metal, the ABE of the perovskite can be systematically changed. Since for *Pm*-3*m* cubic, *Pnma* orthorhombic or $R\bar{3}c$ rhombic perovskite A-site cations are 12-coordinated with oxygen and B-site cations are 6-coordinated with oxygen, the ABE of the perovskite can be calculated based on eq 2, where $\Delta H_{A_mO_n}$ and $\Delta H_{B_mO_n}$ are the heats of formation of A_mO_n and B_mO_n oxides at 298 K, respectively, ΔH_A and ΔH_B are the heats of sublimation of A-metal and B-metal at 298 K, and D_{O_2} is the dissociation energy of gaseous oxygen.[46,47] The electron configuration of B-site transition metal cations is fundamentally the same as that of bulk B-site cations proposed by Bockris and Otagawa[48] (all calculated and experimental results are provided in Table S3).

When we consider ignition, we refer to the point far from equilibrium; thus, the equilibrium vapor pressure of oxygen is not a relevant concept, and we can consider that the valency of the transition metal is invariant and oxygen vacancies are at their theoretical maximum values shown in Table S3.

$$\mathrm{ABE} = \frac{1}{12m}\left(\Delta H_{A_mO_n} - m\Delta H_A - \frac{n}{2}D_{O_2}\right) + \frac{1}{6m}\left(\Delta H_{B_mO_n} - m\Delta H_B - \frac{n}{2}D_{O_2}\right) \quad (2)$$

The ABE of perovskites vs the ignition temperature is shown in Figure 4, which clearly indicates that ignition temperature for Al/perovskite increases with ABE. The most important result when looking at the graph is that the ignition temperature of a thermite reaction is directly correlated to the bond energy of the metal−oxygen bond in the oxidizer. To our knowledge this is the first ever demonstration of this connection.

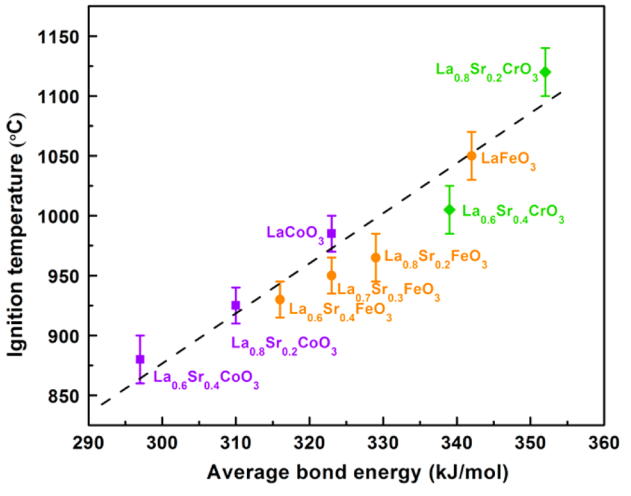

Figure 4. Observed relationship between average bond energy (ABE) of perovskites versus the ignition temperatures of Al/perovskite.

Additionally: (a) Holding δ constant while varying the B-site leads to an ordering of ignition temperature of Cr > Fe > Co and corresponds to the ordering in the ABE. A higher ABE is consistent with an increase in the activation energy for ion migration and thus a decrease in oxygen anion mobility. As discussed previously, Sr^{2+} A-site substitution leads to an elevated oxygen vacancy concentration, δ, resulting from charge balance considerations. (b) Varying δ, through A-site Sr^{2+} substitution, increases vacancies, and thus from eq 1 increases anion conductivity, but also lowers the ABE due to Sr−O being a weaker bond. Again lower ABE is seen to correspond to lower ignition temperature. This trend holds for all samples corresponding to different Sr levels and B-site element. (c) While ABE dominates ignition temperature according to Figure 4, we also note that while Sr^{2+} substitution creates oxygen ion vacancies, it is also changing the ABE. $La_{0.8}Sr_{0.2}FeO_3$ has a higher ABE than $LaCoO_3$ but lower ignition temperature, presumably from a higher oxygen vacancy. This is more clearly defined if we pick a condition where the ABE is held constant but the vacancy concentration is varied. $La_{0.7}Sr_{0.3}FeO_3$ and $LaCoO_3$ have the same nominal ABE, but the former has a slightly lower ignition temperature as seen in Figure 4, consistent with a higher vacancy concentration.

Electronegativity and Ignition Temperature. Previous research has explored the effect of the e_g occupancy of B-site cation and thus metal−oxygen bond's covalency for catalytic activity in oxygen evolution reactions.[49] Thus, electronegativity is another possible metric that could describe the metal−oxygen bond's covalency and energy and relationship to ignition temperature. A more ionic character in an M−O bond should yield a more thermally stable perovskite. This nominally should correspond to a metal with a lower electronegativity.[50] Since both A-site substitution and B-site ions affect the ignition temperature, when analyzing the relationship between electronegativity and ignition temperature, it is necessary to consider the electronegativity of both the A- and B-site cation. In addition, we also have to consider the oxidation state difference between La(III) and Sr(II). When substituting Sr(II) for La(III)'s, the oxidation state has to be normalized from SrO to Sr_2O_2 as in La_2O_3. That is, in the perovskite crystal, Sr(II) is 8-coordinated with oxygen compared to the original La(III), which is 12-coordinated with oxygen.

The formal calculation of the electronegativity is through eq 3

$$\chi = (1 - a)\chi_{La-O} + na\chi_{Sr-O} + \chi_{B-O} \quad (3)$$

where χ is the overall electronegativity difference between cation and oxygen and χ_{La-O}, χ_{Sr-O}, and χ_{B-O} are the electronegativity difference between La, Sr, and B-site atom and oxygen on the Pauling scale,[51] a is the mole fraction of Sr, and n (=2/3) is a factor used to normalize the oxidation state difference between Sr and La.

The larger the electronegativity difference, χ, the high the ionic character in the perovskite and the more stable we should expect the perovskite. Figure 5 clearly shows there exists a trend that ignition temperature increases with increasing electronegativity difference χ in the perovskite and that higher ionic

DOI: 10.1021/acs.jpcc.6b10571
J. Phys. Chem. C 2017, 121, 147−152

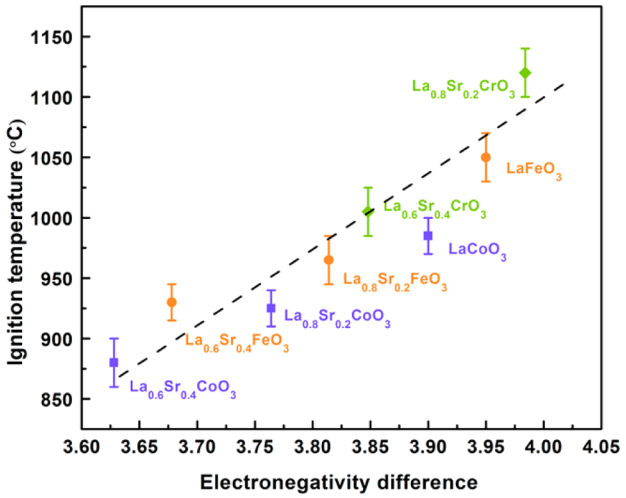

Figure 5. Overall electronegativity difference of perovskites versus ignition temperature of Al/perovskite.

character will increase ignition temperature. Electronegativity offers a potentially simple metric to gauge relative changes in ignition temperature.

CONCLUSIONS

In summary, our study reveals for the first time a clear relationship between molecular properties of the oxidizer and ignition temperature in a thermite reaction. This was enabled by employing a perovskite structure whose crystal structure and particle size could be held constant, but whose vacancy concentration and bond energy could be systematically varied. The results clearly demonstrate that smaller bond energy with smaller electronegativity difference and elevated oxygen vacancy concentration lead to a lower ignition temperature. These results provide important insights into manipulating metal oxides' oxidation properties for thermochemical and energetic applications.

ASSOCIATED CONTENT

Supporting Information

The Supporting Information is available free of charge on the ACS Publications website at DOI: 10.1021/acs.jpcc.6b10571.

Le Bail refinements of XRD, particle size distribution, and T-jump/TOFMS spectra at high heating rate for representative perovskites; SEM of representative thermite particles; listed oxygen release temperature of perovskites and ignition temperature of thermites (PDF)

AUTHOR INFORMATION

Corresponding Author

*E-mail mrz@umd.edu (M.R.Z.).

ORCID

Michael R. Zachariah: 0000-0002-4115-3324

Notes

The authors declare no competing financial interest.

ACKNOWLEDGMENTS

This work was supported by the Army Research Office and the Defense Threat Reduction Agency.

REFERENCES

(1) Goldschmidt, H.; Vautin, T. Reduction of Oxides with Aluminum. *J. Soc. Chem. Ind.* **1898**, *19*, 543.
(2) Dreizin, E. L. Metal-Based Reactive Nanomaterials. *Prog. Energy Combust. Sci.* **2009**, *35*, 141−167.
(3) Zhou, X.; Torabi, M.; Lu, J.; Shen, R.; Zhang, K. Nanostructured Energetic Composites: Synthesis, Ignition/Combustion Modeling, and Applications. *ACS Appl. Mater. Interfaces* **2014**, *6*, 3058−3074.
(4) Apperson, S.; Shende, R. V.; Subramanian, S.; Tappmeyer, D.; Gangopadhyay, S.; Chen, Z.; Gangopadhyay, K.; Redner, P.; Nicholich, S.; Kapoor, D. Generation of Fast Propagating Combustion and Shock Waves with Copper Oxide/Aluminum Nanothermite Composites. *Appl. Phys. Lett.* **2007**, *91*, 243109.
(5) Rossi, C. *Al-Based Energetic Nano Materials: Design, Manufacturing, Properties and Applications*; John Wiley & Sons, Inc.: Hoboken, NJ, 2015.
(6) Yen, N. H.; Wang, L. Y. Reactive Metals in Explosives. *Propellants, Explos., Pyrotech.* **2012**, *37*, 143−145.
(7) Zarko, V. E.; Gromov, A. A. *Energetic Nanomaterials: Synthesis, Characterization, and Application*; Elsevier: Amsterdam, Netherlands, 2016.
(8) Foley, T. J.; Johnson, C. E.; Higa, K. T. Inhibition of Oxide Formation on Aluminum Nanoparticles by Transition Metal Coating. *Chem. Mater.* **2005**, *17*, 4086−4091.
(9) Trunov, M. A.; Schoenitz, M.; Dreizin, E. L. Effect of Polymorphic Phase Transformations in Alumina Layer on Ignition of Aluminum Particles. *Combust. Theory Modell.* **2006**, *10*, 603−623.
(10) Granier, J. J.; Pantoya, M. L. Laser Ignition of Nanocomposite Thermites. *Combust. Flame* **2004**, *138*, 373−383.
(11) Rosenband, V. Thermo-Mechanical Aspects of the Heterogeneous Ignition of Metals. *Combust. Flame* **2004**, *137*, 366−375.
(12) Stamatis, D.; Dreizin, E. L.; Higa, K. Thermal Initiation of Al-MoO_3 Nanocomposite Materials Prepared by Different Methods. *J. Propul. Power* **2011**, *27*, 1079−1087.
(13) Dean, S. W.; Pantoya, M. L.; Gash, A. E.; Stacy, S. C.; Hope-Weeks, L. J. Enhanced Convective Heat Transfer in Nongas Generating Nanoparticle Thermites. *J. Heat Transfer* **2010**, *132*, 111201.
(14) Sullivan, K. T.; Chiou, W. A.; Fiore, R.; Zachariah, M. R. In Situ Microscopy of Rapidly Heated nano-Al and nano-Al/WO_3 Thermites. *Appl. Phys. Lett.* **2010**, *97*, 133104−133106.
(15) Piekiel, N. W.; Egan, G. C.; Sullivan, K. T.; Zachariah, M. R. Evidence for the Predominance of Condensed Phase Reaction in Chemical Looping Reactions Between Carbon and Oxygen Carriers. *J. Phys. Chem. C* **2012**, *116*, 24496−24502.
(16) Piekiel, N. W.; Zhou, L.; Sullivan, K. T.; Chowdhury, S.; Egan, G. C.; Zachariah, M. R. Initiation and Reaction in Al/B_2O_3 Nanothermites: Evidence for the Predominance of Condensed Phase Chemistry. *Combust. Sci. Technol.* **2014**, *186*, 1209−1224.
(17) Wen, J. Z.; Ringuette, S.; Bohlouli-Zanjani, G.; Hu, A.; Nguyen, N.; Persic, J.; Petre, C. F.; Zhou, Y. N. Characterization of Thermochemical Properties of Al Nanoparticle and NiO Nanowire Composites. *Nanoscale Res. Lett.* **2013**, *8*, 184.
(18) Zhou, W.; DeLisio, J. B.; Wang, X.; Egan, G. C.; Zachariah, M. R. Evaluating Free vs Bound Oxygen on Ignition of Nano-Aluminum Based Energetics Leads to a Critical Reaction Rate Criterion. *J. Appl. Phys.* **2015**, *118*, 114303.
(19) Jian, G.; Chowdhury, S.; Sullivan, K.; Zachariah, M. R. Nanothermite Reactions: Is Gas Phase Oxygen Generation from the Oxygen Carrier an Essential Prerequisite to Ignition? *Combust. Flame* **2013**, *160*, 432−437.
(20) Trunov, M. A.; Schoenitz, M.; Zhu, X.; Dreizin, E. L. Effect of Polymorphic Phase Transformations in Al_2O_3 Film on Oxidation Kinetics of Aluminum Powders. *Combust. Flame* **2005**, *140*, 310−318.
(21) Levitas, V. I.; Asay, B. W.; Son, S. F.; Pantoya, M. L. Melt Dispersion Mechanism for Fast Reaction of Nanothermites. *Appl. Phys. Lett.* **2006**, *89*, 071909.

DOI: 10.1021/acs.jpcc.6b10571
J. Phys. Chem. C 2017, 121, 147−152

(22) Huang, Y. H.; Dass, R. I.; Xing, Z. L.; Goodenough, J. B. Double Perovskites as Anode Materials for Solid-Oxide Fuel Cells. *Science* **2006**, *312*, 254−257.
(23) Laguna-Bercero, M. A.; Kilner, J. A.; Skinner, S. J. Performance and Characterization of (La, Sr) MnO_3/YSZ and $La_{0.6}Sr_{0.4}Co_{0.2}Fe_{0.8}O_3$ Electrodes for Solid Oxide Electrolysis Cells. *Chem. Mater.* **2009**, *22*, 1134−1141.
(24) Dai, X. P.; Wu, Q.; Li, R. J.; Yu, C. C.; Hao, Z. P. Hydrogen Production from a Combination of the Water-Gas Shift and Redox Cycle Process of Methane Partial Oxidation via Lattice Oxygen over $LaFeO_3$ Perovskite Catalyst. *J. Phys. Chem. B* **2006**, *110*, 25856−25862.
(25) Schiestel, T.; Kilgus, M.; Peter, S.; Caspary, K. J.; Wang, H.; Caro, J. Hollow Fiber Perovskite Membranes for Oxygen Separation. *J. Membr. Sci.* **2005**, *258*, 1−4.
(26) Hallberg, P.; Jing, D.; Rydén, M.; et al. Chemical Looping Combustion and Chemical Looping with Oxygen Uncoupling Experiments in a Batch Reactor Using Spray-Dried $CaMn_{1-x}M_xO_{3-\delta}$ (M = Ti, Fe, Mg) Particles as Oxygen Carriers. *Energy Fuels* **2013**, *27*, 1473−1481.
(27) Liu, L.; Taylor, D. D.; Rodriguez, E. E.; Zachariah, M. R. Influence of Transition Metal Electronegativity on the Oxygen Storage Capacity of Perovskite Oxides. *Chem. Commun.* **2016**, *52*, 10369−10372.
(28) Jian, G.; Liu, L.; Zachariah, M. R. Facile Aerosol Route to Hollow CuO Spheres and Its Superior Performance as an Oxidizer in Nanoenergetic Gas Generators. *Adv. Funct. Mater.* **2013**, *23*, 1341−1346.
(29) Cheary, R. W.; Coelho, A. A. Fundamental Parameters Approach to X-Ray Line-Profile Fitting. *J. Appl. Crystallogr.* **1992**, *25*, 109−121.
(30) Zhou, L.; Piekiel, N.; Chowdhury, S.; Zachariah, M. R. T-Jump/Time-of-Flight Mass Spectrometry for Time-Resolved Analysis of Energetic Materials. *Rapid Commun. Mass Spectrom.* **2009**, *23*, 194−202.
(31) Jian, G.; Piekiel, N. W.; Zachariah, M. R. Time-Resolved Mass Spectrometry of Nano-Al and Nano-Al/CuO Thermite under Rapid Heating: A Mechanistic Study. *J. Phys. Chem. C* **2012**, *116*, 26881−26887.
(32) Chowdhury, S.; Sullivan, K.; Piekiel, N.; Zhou, L.; Zachariah, M. R. Diffusive vs Explosive Reaction at the Nanoscale. *J. Phys. Chem. C* **2010**, *114*, 9191−9195.
(33) Muller, O.; Roy, R. *The Major Ternary Structural Families*; Springer: Berlin, 1974.
(34) Liu, L.; Zachariah, M. R.; Stoliarov, S. I.; Li, J. Enhanced Thermal Decomposition Kinetics of Poly (Lactic Acid) Sacrificial Polymer Catalyzed by Metal Oxide Nanoparticles. *RSC Adv.* **2015**, *5*, 101745−101750.
(35) Zhou, L.; Piekiel, N.; Chowdhury, S.; Zachariah, M. R. Time-Resolved Mass Spectrometry of the Exothermic Reaction between Nanoaluminum and Metal Oxides: the Role of Oxygen Release. *J. Phys. Chem. C* **2010**, *114*, 14269−14275.
(36) Cherry, M.; Islam, M. S.; Catlow, C. R. A. Oxygen Ion Migration in Perovskite-Type Oxides. *J. Solid State Chem.* **1995**, *118*, 125−132.
(37) Ishihara, T.; Matsuda, H.; Takita, Y. Doped $LaGaO_3$ Perovskite Type Oxide as a New Oxide Ionic Conductor. *J. Am. Chem. Soc.* **1994**, *116*, 3801−3803.
(38) Teraoka, Y.; Nobunaga, T.; Yamazoe, N. Effect of Cation Substitution on the Oxygen Semipermeability of Perovskite-Type Oxides. *Chem. Lett.* **1988**, *17*, 503−506.
(39) Stevenson, J. W.; Armstrong, T. R.; Carmeim, R. D.; Pederson, L. R.; Weber, L. R. Electrochemical Properties of Mixed Conducting Perovskites La_{1-x} M_xCo_{1-y} $Fe_yO_{3-\delta}$ (M = Sr, Ba, Ca). *J. Electrochem. Soc.* **1996**, *143*, 2722.
(40) Nemudry, A.; Weiss, M.; Gainutdinov, I.; Boldyrev, V.; Schöllhorn, R. Room Temperature Electrochemical Redox Reactions of the Defect Perovskite $SrFeO_{2.5+x}$. *Chem. Mater.* **1998**, *10* (9), 2403−2411.
(41) Piercey, D. G.; Klapoetke, T. M. Nanoscale Aluminum-Metal Oxide (Thermite) Reactions for Application in Energetic Materials. *Cent. Eur. J. Energy Mater.* **2010**, *7*, 115−129.
(42) Puszynski, J. A.; Bulian, C. J.; Swiatkiewicz, J. J. Processing and Ignition Characteristics of Aluminum-Bismuth Trioxide Nanothermite System. *J. Propul. Power* **2007**, *23*, 698−706.
(43) Zhao, H.; Xu, N.; Cheng, Y.; Wei, W.; Chen, N.; Ding, W.; Lu, X.; Li, F. Investigation of Mixed Conductor $BaCo_{0.7}Fe_{0.3-x}Y_xO_{3-\delta}$ with High Oxygen Permeability. *J. Phys. Chem. C* **2010**, *114*, 17975−17981.
(44) Sammells, A. F.; Cook, R. L.; White, J. H.; Osborne, J. J.; Macduff, R. C. Rational Selection of Advanced Solid Electrolytes for Intermediate Temperature Fuel Cells. *Solid State Ionics* **1992**, *52*, 111−123.
(45) Cook, R. L.; Sammells, A. F. On the Systematic Selection of Perovskite Solid Electrolytes for Intermediate Temperature Fuel Cells. *Solid State Ionics* **1991**, *45*, 311−321.
(46) Li, S.; Jin, W.; Huang, P.; Xu, N.; Shi, J.; et al. Comparison of Oxygen Permeability and Stability of Perovskite Type $La_{0.2}A_{0.8}Co_{0.2}Fe_{0.8}O_{3-\delta}$ (A= Sr, Ba, Ca) membranes. *Ind. Eng. Chem. Res.* **1999**, *38*, 2963−2972.
(47) Lide, D. R. Standard Thermodynamic Properties of Chemical Substances. In *CRC Handbook of Chemistry and Physics*; CRC Press: 2007; Vol. 5.
(48) Bockris, J. O. M.; Otagawa, T. The Electrocatalysis of Oxygen Evolution on Perovskites. *J. Electrochem. Soc.* **1984**, *131*, 290−302.
(49) Suntivich, J.; May, K. J.; Gasteiger, H. A.; Goodenough, J. B.; Shao-Horn, Y. A Perovskite Oxide Optimized for Oxygen Evolution Catalysis from Molecular Orbital Principles. *Science* **2011**, *334*, 1383−1385.
(50) Ramam, K.; Chandramouli, K. Dielectric and Piezoelectric Properties of Combinatory Effect of A-Site Isovalent and B-Site Acceptor Doped PLZT Ceramics. *Ceram. Silikaty* **2009**, *53*, 189−194.
(51) Pauling, L. The Nature of the Chemical Bond. IV. The Energy of Single Bonds and the Relative Electronegativity of Atoms. *J. Am. Chem. Soc.* **1932**, *54*, 3570−3582.

DOI: 10.1021/acs.jpcc.6b10571
J. Phys. Chem. C 2017, 121, 147−152